The Oslo Model

Ilaria Manco
CID: 00938658

Abstract

Numerical simulations of the boundary-driven Oslo Model were performed in order to investigate the self-organised criticality of the cellular automaton describing a one-dimensional stochastic ricepile by proposing and verifying a series of finite-size scaling ansatz for the height field, the height probability and the avalanche-size probability.
The height of the pile was studied in terms of transient and recurrent configurations and corrections to scaling were found for some of the observables showing finite-size signatures; the avalanche-size critical exponents were found to be $\tau_s = 1.55$ *and* $D = 2.23$*, close to the widely accepted values for the OM model [3]. A data collapse analysis was devised in all the cases and, additionally, a moment analysis was carried out to estimate the avalanche-size exponents.*

Word Count: ≈ 2580 word

1. INTRODUCTION

Self-organised criticality (SOC), first introduced by Bak et al., is a property of a slowly-driven non-equilibrium system with extended degrees of freedom that *naturally evolves into a self-organised critical point* [1], thus showing scale invariance without any external fine-tuning of control parameters.

The archetypical example of such a system is the slowly-driven sandpile organising itself into a highly susceptible state where its slope fluctuates around a constant angle of repose. An analogous behaviour is also exhibited by other real granular media, like rice, to study which the Oslo Model (OM) was developed as a cellular automaton describing the slowly-driven one-dimensional ricepile [2].

Applications of the SOC paradigm, however, extend well beyond the realm of granular media and include other natural systems (earthquakes, precipitation, biological networks) as well as systems in human sciences like economics.

1.1 The model

Here, the algorithm of the boundary-driven OM, as described by Christensen et al. [3], is implemented in Python with the aim of studying the ricepile model within the finite-size scaling theory and extrapolating the critical exponents.

The systems were modelled on a one-dimensional finite lattice of size $L \in \{8, 16, 32, 64, 128, 256\}$ and, given the finiteness of the simulation, careful consideration was taken when dealing with the observables of interest and, in some cases a quantitative estimate of the correction to scaling was found.

In the first half of the report, an investigation of the height field $h(t; L)$ is presented, while the second part focuses on the avalanche size s, for which the relevant scaling exponents were evaluated from its probability density function and with use of the moment analysis technique.

For the purpose of this report, the definitions of time and number of grains added are equivalent, given the discreteness of the model.

Results were obtained from numerical simulations by collecting measurements of the observables of interest (h, s, d) at any time t using an end time $t = 10^6$.

Numerical analysis was then performed to extract critical exponents and corrections to scaling. These results were then corroborated by performing a data collapse of the relevant quantities.

2. HEIGHT OF THE PILE

2.1 Transient and recurrent configurations

For a system in a stable configuration, i.e. when the local slope $z_i \leq z_i^{th}$ (the local threshold slope) for all sites i, at a given time t, the height of the pile $h(t; L)$ is defined as

$$h(t; L) = \sum_{i=1}^{L} z_i \qquad (1)$$

Each time it undergoes relaxation, the system evolves into one of the 3^L stable configurations [3]. Some of these are at most encountered once (transient) but, after a sufficiently high number of iterations, the system self-organises into a set $\mathcal{R}$ of recurrent configurations, called the attractor of the dynamics [3] where the average height $\langle h \rangle$ fluctuates around a constant value.

During the transient time, the height profile is then increasing independently of the system size L (Fig. 1), since no grain has yet left the system and therefore the number of iterations equals the number of grains in the pile.

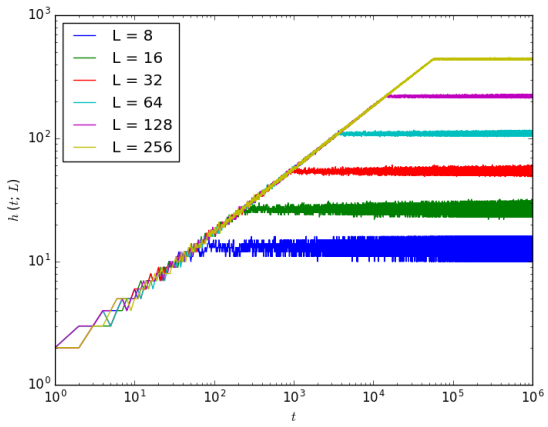

Figure 1. Log-log plot of the time-development of the height field. Below the size-dependent crossover time t_c, all the curves fall onto a common straight line; after t_c they reach a plateau value dependent on the system size L.

Consequently, the time it takes for a system to enter the set $\mathcal{R}$ of recurrent configurations, which occurs when a grain first leaves the site $i = L$, is bounded between two limiting cases:

a) $if\ \forall\ i\colon\ z_i^{th} = 1\ \Rightarrow\ t_c(L) = \frac{L\,(L+1)}{2}$

b) $if\ \forall\ i\colon\ z_i^{th} = 2\ \Rightarrow\ t_c(L) = L(L+1)$

and the crossover time $t_c(L) \propto L^2$ in the thermodynamic limit $L \to \infty$.

Following the same reasoning, once the system has reached the steady state, the height of the pile can take up values between two boundaries:

$$L < h < 2L.$$

Hence, we expect the height to scale linearly with system size.

2.2 Height – Scaling Ansatz

As evident from Fig. 1, in the transient period the height of the pile follows a power law with a cutoff at $t = t_c$ that diverges with system size, clearly indicating scale invariance in the system. It then ceases to grow and fluctuates around a mean value $\tilde{h}$ which is only dependent on L.
On this basis, we can therefore propose a finite-size scaling ansatz for the moving average height of the pile:

$$\tilde{h}(\mathrm{t};\mathrm{L}) \propto L^{\alpha}\,\mathcal{F}\left(\frac{t}{t_c}\right) \tag{2a}$$

$$t_c \propto L^{\beta}, \tag{2b}$$

where α and β are finite size scaling exponents and the scaling function is consistent with the form

$$\mathcal{F}\left(\frac{t}{t_c}\right) \propto \begin{cases} \left(\frac{t}{t_c}\right)^{\gamma}, & t < t_c \\ constant, & t > t_c \end{cases} \tag{3}$$

By choosing $\gamma = 0.5$, the size dependence is therefore cancelled out for small arguments, while the time dependence vanishes in the asymptotic regime; the scaling exponents α and β can be found by plotting $\tilde{h}$ in the steady state and t_c against L respectively (Sec 2.3).
Fig. 2 illustrates the scaling behaviour of the critical time t_c, from which β was determined to be equal to 2.04.

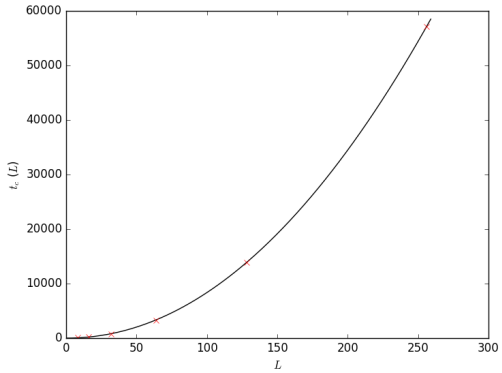

Figure 2. Relationship between the critical time $t_c(L)$ for the various system sizes considered. This was found by imposing a bound on the increase of the moving average and determining when the power law trend of the law ceased to occur.

By attempting a data collapse of the height for different system sizes onto a single curve, we obtain a convincingly good graph.

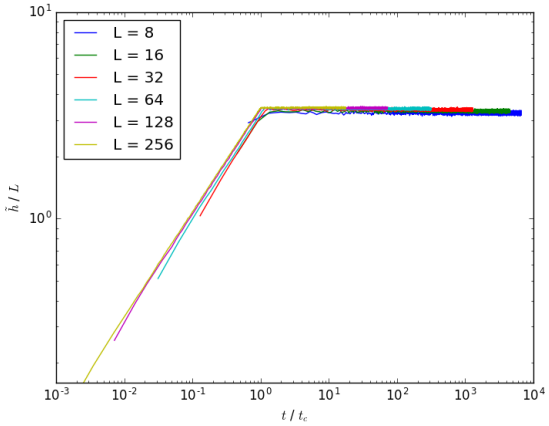

Figure 3. Attempted collapse of the processed height $\tilde{h}(t;L)$ (log-log scale). The x-axis was rescaled by plotting t/t_c, while on the y-axis the transformed height $\tilde{h}(t;L)/L$ was plotted, hence assuming $\alpha = 1$. This shows a good data collapse, although small deviations are observed for the small L.

2.3 Height – correction to scaling

In order to extract the finite size scaling exponent α, the time-average of the height in the steady state was found as follows:

$$\langle h(t;L)\rangle = \lim_{T\to\infty}\frac{1}{T}\sum_{t=\,t_0+1}^{t_0+T} h\,(t;\,L) \tag{4}$$

where $t_0 > t_c\,(L)$.

This quantity was plotted as a function of system size L (Fig. 4); a linear regression fit of these two quantities confirmed the numerical result $\alpha = 1.00$, and delivered an estimation of the constant

of proportionality $a_0 \approx 1.72$, later discussed in more detail.

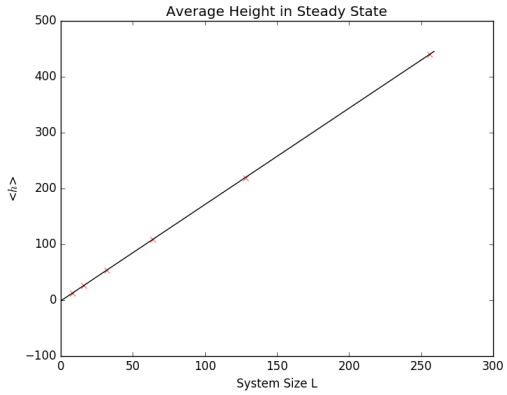

Figure 4 The linear relationship between the average height $\langle h(t;L)\rangle$ and the system size L. The slope found from linear regression is $a_0 \approx 1.72$.

However, a plot of the ratio $\langle h\rangle/L$ (Fig. 5) against the log-scaled system sized revealed a deviation from the expected constant value for small system sizes, suggesting that, the linear scaling of the average height holds only for sufficiently big system sizes L.

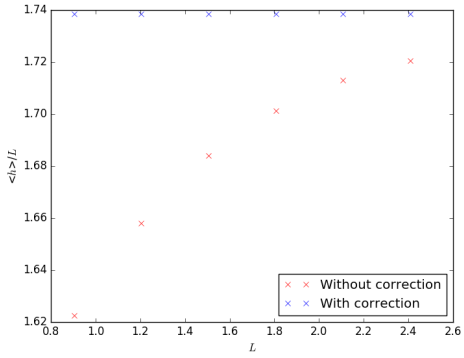

Figure 5. Scaling of the $\langle h\rangle/L$ ratio against the system size on a logarithmic scale. Under the assumption of a linear relationship between $\langle h\rangle$ and L, this would be expected to give a straight line. However, finite-size effects are detectable for small L and, by applying corrections to scaling, the linear relationship is recovered.

It is therefore necessary to introduce some correction to scaling of the following form:

$$\langle h\,(t;L)\rangle = a_0 L\,(1 - a_1 L^{-\omega_1} + a_2 L^{-\omega_2} + \cdots), \tag{5}$$

where a_i and ω_i are constants.

Neglecting terms with $i > 1$, the correction constants a_0 and ω_1 can be estimated by rearranging Eq. (5) into the form

$$\log\left(\frac{\langle h\rangle}{L} - a_0\right) = -\omega_1 \log L + \log(a_0 a_1) \tag{6}$$

and finding the value of a_0 for which a straight line results from the plot of the left-hand side of Eq. (6) against L and extracting the value of its slope, corresponding to ω_1.
From this, numerical results were obtained, giving $a_0 = 1.73 \pm 0.01$ and $\omega_1 = 0.55 \pm 0.01$.
Accordingly, we conclude that the fluctuations in $\langle h\,(t;L)\rangle$ due to small system size L scale sublinearly with L [5].

In order to investigate the fluctuations in the height profile (profile width [4]) of the pile once the system has reached the attractor of the dynamics, an observable of particular interest is the standard deviation of the height, defined as

$$\sigma_h(L) = \sqrt{\langle h^2\,(t;L)\rangle - \langle h\,(t;L)\rangle^2}. \tag{7}$$

A plot of this quantity on a logarithmic scale (Fig. 6) provides a visual representation of its scaling relation with the system size L:

$$\sigma_h(L) \propto L^{\chi}, \tag{8}$$

and yields a value for the finite size scaling exponent $\chi = 0.24 \pm 0.01$.

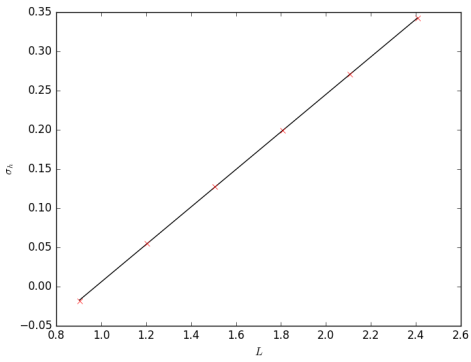

Figure 6 The relationship between the standard deviation of the height $\sigma_h(L)$ and the system size L (on a log-log scale). The slope found from linear regression is $\chi \approx 0.24$.

Signatures of corrections to scaling would in principle be expected to emerge from the plot of the ratio $\sigma_h(L)/L$. However, these are in practice hard to detect in our simulation, due to large statistical uncertainties.

Given the definition of the average slope of the pile at time t as

$$z\,(t;\,L) = \frac{1}{L}\sum_{i=1}^{L} z_i = \frac{1}{L}\,h\,(t;L), \qquad (9)$$

it is interesting to notice that, in the asymptotic limit of infinite system size L, this tends towards the constant value a_0 and its standard deviation $\sigma_z(L)$, which scales according to $L^{\chi-1}$, converges to 0.

2.4 Height probability

From the analysis of the average height and its standard deviation, we have found that both quantities displayed scaling behaviour with respect to the system size. Therefore, it is reasonable to assume that a data collapse will be possible for the height probability, thereby confirming the validity of the scaling ansatz of Eq. (2).

The height probability was numerically calculated for all system sizes L (Fig. 7) following the definition:

$$P(h;L) = \frac{No.\ of\ observed\ configurations\ with\ height\ h}{Total\ no.\ of\ observed\ configurations}$$

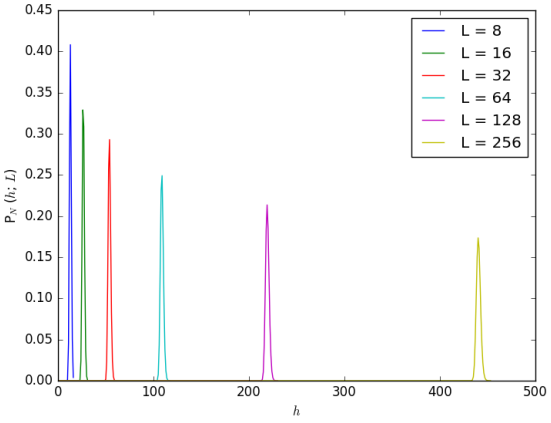

Figure 7 Individual height probabilities $P(h;L)$ for the range of system sizes $L \in \{8, 16, 32, 64, 128, 256\}$. These clearly follow (at least to a certain approximation) a Gaussian shape, peaking at the average height ⟨h (t;L)⟩ previously found.

As shown in Fig. 5, the height probability can be closely approximated by a Gaussian:

$$P\,(h;L) = \frac{1}{\sigma_h\sqrt{2\,\pi}}\,e^{-\frac{(h-\langle h\rangle)^2}{2\,\sigma_h^2}} \qquad (10)$$

and, as such, can be subject to a data collapse, by rescaling it into the transformed probability $\sigma_h P(h;L)$ and plotting it against $\frac{h-\langle h\rangle}{\sigma_h}$, where $h - \langle h\rangle$ represents the rescaled height (Fig. 8).

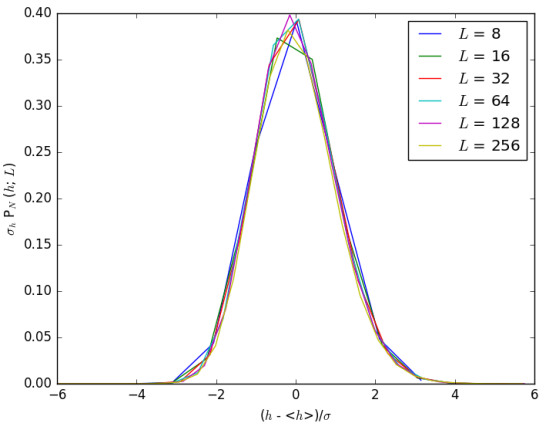

Figure 8 Attempted data collapse for the height probability $P(h;L)$. The transformed probability $\sigma_h P(h;L)$ was plotted against the rescaled height $\frac{h-\langle h\rangle}{\sigma_h}$ and the result shows a good agreement with the scaling ansatz in Eq. (10).

3. AVALANCHE-SIZE PROBABILITY

In the boundary-driven OM, each time the external drive triggers the threshold, an interaction occurs between neighbouring sites in the form of toppling, initiating a relaxation mechanism that follows stochastic rules.

The totality of relaxation events is called an avalanche and its size is determined by the number of topplings caused by one drive, including cases when this is 0, for the purpose of a correct normalisation.

Again considering exclusively systems in their steady state ($t > t_c$), the probability of observing an avalanche of size s in a system of size L can be computed as

$$P_N(s;L) = \frac{No.\ of\ avalanches\ of\ size\ s}{Total\ no.\ of\ avalanches\ N}$$

.

3.1 Data binning

Due to the intrinsic limitations of finite statistics, the raw output of the probability density $P_N(s;L)$ computed from our data sets as stated above suffers from significant noise even for the largest samples ($N = 10^6$), owing to its power law behaviour (Fig. 9).

As a result, it would be computationally prohibitive to adequately extract the underlying behaviour from the raw PDF and a logarithmic binning of the data from the largest sample ($N = 10^6$) is therefore necessary [3].
Care was taken in determining an appropriate growth factor a by which consecutive bins increase in size, so that it was high enough to mask the statistical noise without excessively smoothing out the data. Values from 1.1 to 2.0 were tested in steps of 0.1 and a value of $a = 1.4$ was chosen as the most suitable.

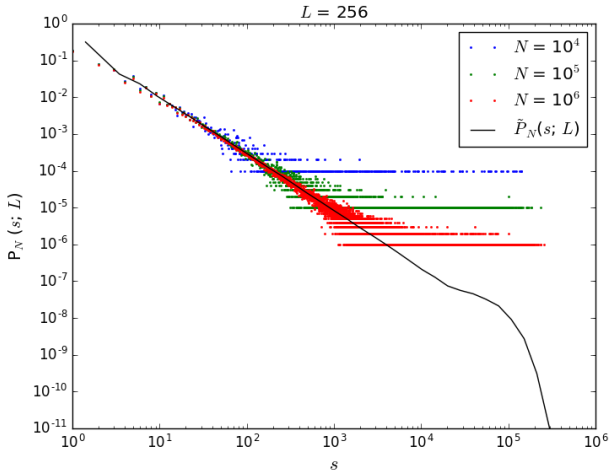

Figure 9 Raw avalanche-size probability $P_N(s;L)$ (dots) calculated in a range of total no. of avalanches $N \in \{10^4, 10^5, 10^6\}$ and log-binned probability $\tilde{P}_N(s;L)$ (line) for the system size $L = 256$ with $N = 10^6$. The tail of the unprocessed distribution displays significant statistical noise even for the largest N, while processing the data using a log-binning procedure reveals the underlying behaviour, characterised by an upper cutoff.

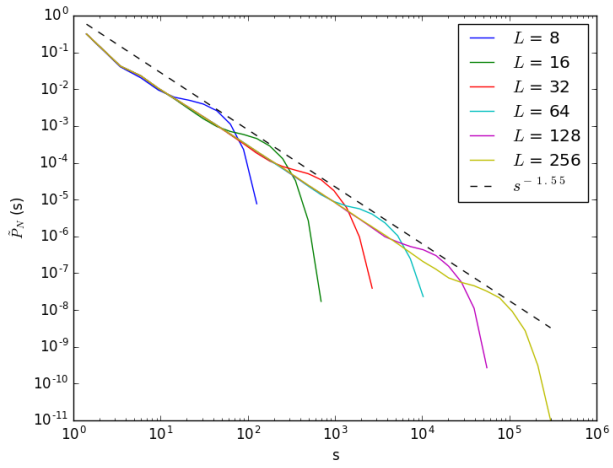

Figure 10 Processed numerical results for the probability $\tilde{P}_N(s;L)$ for all system sizes L versus the avalanche size s. The frequency of avalanches decays with size. The dashed line corresponds to the slope (on a logarithmic scale) of the probability distribution away from the cutoff versus s, identified with the avalanche-size exponent τ_s.

The data binned following this procedure is presented above in Fig. 10. As displayed in the plot, no typical size of an avalanche exists other than a cutoff avalanche size, s_c, increasing with system size. As a result, a rescaling of the observable s and the system's parameter L allows us to probe for the scaling symmetry of the systems.

3.2 Avalanche-size probability - Scaling ansatz

Following the observations provided in the previous section, we expect the processed avalanche-size probability density function $\tilde{P}_N(s;L)$ to follow a scaling law of the form

$$\tilde{P}_N(s;L) \propto s^{-\tau_s}\mathcal{G}(s/s_c) \quad (11a)$$

$$s_c \propto L^D \quad (11b)$$

for $L \gg 1$, $s \gg 1$, where τ_s is the avalanche-size exponent and D is called the avalanche dimension, which establishes the divergence of the maximum size distribution with system size and is therefore a finite size exponent, thereby subject to corrections to scaling, as previously seen for the height field (Sec. 2.3).

An estimation of τ_s can easily be carried out, within a limited accuracy, via a linear fit of the intermediate section of the PDF away from the cutoff ($1 \ll s \ll s_c$), here chosen to be $10^1 < s < 10^4$ for the system size $L = 256$.
Following this procedure, the critical exponent was estimated to be $\tau_s \approx 1.55$.

Determining the upper cutoff $s_c(L)$ from the probability density, however, results more challenging and requires a more careful consideration: this upper bound on the avalanche size is imposed by the finite size of the system; in the steady state, the total number of grains scales as L^2 and the biggest avalanche would occur if all the grains were dissipated; for a grain to drop out of the system, this needs to topple a maximum number of times equal to L, thus giving $s_c(L) < L^3$. Hence we expect $D < 3$.

A simple procedure to extract the upper cutoff was followed here from a calculation of the values corresponding to the tail of the bumps (Fig. 10). These were used as a rough estimation of $s_c(L)$, by effectively identifying the upper cutoff with the maximum event size recorded in the sample, and a logarithmic plot of $s_c(L)$ against system size L revealed a value of $D \approx 2.20$.
This estimation suffers however from significant statistical uncertainty, as it is heavily dependent on the sample size and increases for large avalanche sizes due to its dependence on the increasing bin size (Sec. 3.1).
Therefore this provides a reasonable explanation for its deviation from the expected value $D = 2.25$.

Furthermore, it is interesting to notice that the rescaled plot in Fig. 10 reveals a striking feature for small avalanche sizes that signals the presence of a lower cutoff, below which, the PDF ceases to follow a universal behaviour [6].

As seen, an analysis of the avalanche-size probability density is of primary importance in the path to a complete understanding of how scale invariance arises in SOC models.
However, the accuracy of the results thus obtained is limited by the presence of a lower and upper cutoff in the distribution, which makes the extrapolation of the local slope of the distribution (and its intercept) subject to considerable uncertainty.

3.4 Scaling relations

A relationship between the two critical exponents τ_s and D exists and can be derived from the average avalanche size

$$\langle s \rangle = \sum_{s=1}^{\infty} s\, \tilde{P}_N(s; L) \tag{12a}$$

$$\langle s \rangle \approx \int_1^{\infty} s^{-\tau_s+1}\, \mathcal{G}\,(s/L^D)\; ds, \tag{12b}$$

where we have approximated the sum in Eq. (12a) to an integral and assumed that this is valid for all avalanche sizes.

Since $\mathcal{G}\,(s/L^D)$ decays rapidly enough (the ratio $s/s_c \to 0$ for large system sizes) and $\tau_s < 2$, the integral converges for both the upper and lower limits and, making use of the substitution $s/L^D = u$, Eq. (12b) becomes

$$\langle s \rangle \propto L^{D(2-\tau_s)}. \tag{13}$$

Once the system has reached the set of recurrent configurations, the pile does not grow further and every grain added is dissipated (Sec. 2.1) after toppling a number of times of the order of L. Hence we can argue that $\langle s \rangle \propto L$ and we can thus derive the scaling relation:

$$D(2 - \tau_s) = 1. \tag{14}$$

The estimation of the universal exponents from the inspection of the PDF only loosely satisfies the above scaling relation and, indeed, this is expected as a direct analysis of the probability mainly provides a qualitative assessment of the scaling hypothesis [6] and is, as a consequence, insufficient for a quantitatively satisfactory treatment.

3.5 Moment Analysis

In addition to the evaluation of the critical exponents via the probability density function, it is often advantageous to conduct a moment analysis in order to obtain more accurate values [7].

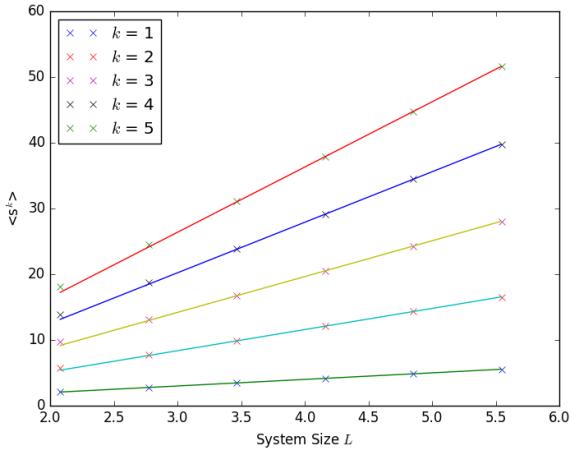

Figure 11. K[th] moments $\langle s^k \rangle$ (k = 1, 2, 3, 4, 5) versus the system size L . The slope of each line is the estimate of d log$\langle s^k \rangle$/d log$L$

The k[th] moment is defined as

$$\langle s^k \rangle = \lim_{T \to \infty} \frac{1}{T} \sum_{t=t_0+1}^{t_0+T} s_t^k, \qquad (15)$$

where s_t is the measured avalanche size at time t in the steady state.

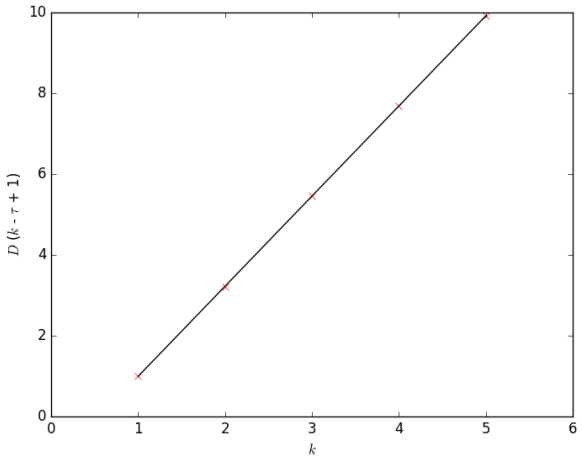

Figure 13. The estimated exponent $D(1-\tau_s+k)$ versus the moment k. The slope of the straight line was found to be D = *2.23* and the intersection was determined to be at y = - 1.24, implying τ_s = 1.556.

In analogy to the derivation of the scaling relation in Sec. 3.4, the k[th] moment is expected to scale with system size as follows

$$\langle s^k \rangle \propto L^{D(1-\tau_s+k)}, \qquad (16)$$

from which it is easy to see that a linear regression can be used to estimate the universal exponents τ_s and D.

A logarithmic plot (Fig. 12) of a range of moments $k \in \{1, 2, 3, 4, 5\}$ against the range of system sizes therefore enables us to estimate the scaling exponents, on the basis of the relation in Eq. (16).

This yields a result of τ_s = 1.55 ± 0.01 and D = 2.23 ± 0.01, in higher agreement with the widely accepted values (τ_s = 1.55 and D = 2.25) [3] when the two smallest system sizes are not included in the linear regression in order to account for corrections to scaling emerging when dealing with small L.

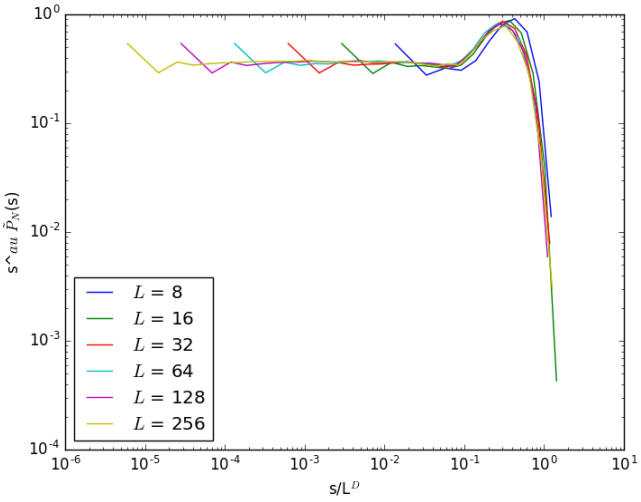

Figure 12 Data collapse of the avalanche-size PDF obtained using τ= 1.55 and D = 2.23

As a final confirmation of the validity of the FFS, a complete data collapse for the PDF, shown in fig. 13 was produced using the exponents found as described above.

5. CONCLUSION

Numerical simulations of the boundary-driven one-dimensional Oslo Model were performed with the purpose of investigating the scaling behaviour of the model and extracting the characteristic exponents and factors, together with a numerical estimation of the corrections to scaling necessary for the precise extrapolation of any finite size scaling (FSS) exponent (and function).

The FSS hypothesis was tested for several observables of interest (height of the pile, height probability, avalanche-size probability) through data collapses of the relevant quantities; in addition, a moment analysis was carried out to more accurately estimate the avalanche-size exponents.

The finiteness of the lattice was consistently found to constitute the only scale governing the statistics of the observables and small perturbations were observed to induce catastrophic events involving the entire system, thus revealing spatiotemporal correlations underlying the system, as typically observed in SOC.

Despite the limited sample size and the relatively small system sizes examined (up to $L = 256$), the OM model was found to coherently describe the behaviour of slowly-driven granular systems within the finite-size scaling framework, although the large statistical uncertainties did not allow to achieve the same accuracy as in studies considering larger simulations.

REFERENCES

[1] P. Bak, C. Tang, K. Wiesenfeld. Self-Organized Criticality: An Explanation of 1/f Noise. *Phys. Rev. Lett.* 1987; 59(4): 381-384. [Online] Available from: doi: https://doi.org/10.1103/PhysRevLett.59.381 [Accessed 19th February 2017]

[2] K. Christensen, Á. Corral, V. Frette, J. Feder, T. Jøssang Tracer Dispersion in a Self-Organized Critical System. *Phys. Rev. Lett.* 77(1): 107. [Online] Available from: doi: https://doi.org/10.1103/PhysRevLett.77.107 [Accessed 19th February 2017]

[3] K. Christensen, N. R. Moloney. *Complexity and Criticality*. London: Imperial College Press; 2005

[4] A. Malthe-Sørenssen, J. Feder, K. Christensen, V. Frette, T. Jøssang. Structure and Dynamics of the Surface in a Pile of Rice. [Preprint] 2001. Available from: http://www.cmth.ph.ic.ac.uk/people/k.christensen/papers/preprints/preprint_pre_2001.pdf [Accessed 19th February 2017]

[5] P. Pradhan and D. Dhar. Sampling rare fluctuations of height in the Oslo ricepile model. *J. Phys. A*. 2007; 40(11). [Online] Available from: doi: 10.1088/1751-8113/40/11/003 [Accessed 19th February 2017]

[6] G. Pruessner. *Self-Organised Criticality: Theory, Models and Characterisation*. Cambridge: Cambridge University Press; 2012.

[7] Z. Duan-Ming et al. Moment Analysis of a Rice-Pile Model. *Commun. Theor. Phys*. 2005; 43(5): 483-486. Available from: doi: https://doi.org/10.1088/0253-6102/43/3/021 [Accessed 19th February 2017]